# Anisotropic dressing of electrons in electron-doped cuprate superconductors

Shuning Tan, Yiqun Liu, Yingping Mou, and Shiping Feng ◉*
*Department of Physics, Beijing Normal University, Beijing 100875, China*

Recent experiments revealed a remarkable possibility for the absence of the disparity between the phase diagrams of electron- and hole-doped cuprate superconductors, while such an aspect should also be reflected in the dressing of the electrons. Here the phase diagrams of electron-doped cuprate superconductors and the related exotic features of the anisotropic dressing of the electrons are studied based on kinetic-energy-driven superconductivity. It is shown that although the optimized $T_c$ in the electron-doped side is much smaller than that in the hole-doped case, the electron- and hole-doped cuprate superconductors rather resemble each other in the doping range of the superconducting dome, indicating an absence of the disparity between the phase diagrams of electron- and hole-doped cuprate superconductors. In particular, the anisotropic dressing of the electrons due to strong electron coupling to strongly dispersive spin excitation leads to the truncation of the electron Fermi surface to form the disconnected Fermi arcs centered around the nodal region. Concomitantly, the dip in the peak-dip-hump structure of the quasiparticle excitation spectrum is directly associated with the corresponding peak in the quasiparticle scattering rate, while the dispersion kink is always accompanied by the corresponding inflection point in the total self-energy as the dip in the peak-dip-hump structure and the dispersion kink in the hole-doped counterparts. The theory also predicts that both normal and anomalous self-energies exhibit well-pronounced low-energy peak structures.

## I. INTRODUCTION

The parent compound of cuprate superconductors is classified as a half-filled Mott insulator with antiferromagnetic (AF) long-range order (AFLRO) [1,2], which is due to the very strong electron correlation [3]. In the hole-doped case [1], a small number of the doped holes destroys AFLRO quickly, and then superconductivity appears leaving only the AF short-range order (AFSRO) correlation still intact [4–7]. However, in the electron-doped side [2], both the doped electrons and the annealing process in a low-oxygen environment are required to induce superconductivity, where the early experimental observations [8–14] revealed that in clear contrast to the hole-doped case, AFLRO survives until superconductivity appears only in a narrow window of the highly doped electrons, around the optimal doping, and it can persist into the superconducting (SC) phase. In particular, a large pseudogap opens at around the crossing points of the electron Fermi surface (EFS) with the AF Brillouin zone boundary due to the AFLRO correlation [8–14]. Moreover, unlike the universal domelike shaped doping dependence of the SC transition temperature $T_c$ in the hole-doped case [5–7] with an optimal doping at around 15%, the SC phase in the electron-doped side shows a large variation [8]. This disparity between the phase diagrams of the electron- and hole-doped cuprate superconductors implies that the electron doping and hole doping may affect the electronic structure in different ways [5–14].

Since the additional annealing process is crucial for realizing superconductivity in the electron-doped side [8–14], the different annealing methods may result in distinct properties, reflecting the fact that the controversy of the phase diagram in the electron-doped side may be attributed to the conflicting experimental results associated with the annealing effect. Although the effect of the annealing is still not fully understood on a microscopic level [15,16], it is possible that the intrinsic aspects of the electron-doped cuprate superconductors are masked by the improper annealing condition. Recently, substantial improvements in the materials synthesis technique [16–20] have enabled the single crystals of the electron-doped cuprate superconductors to be grown in the optimal annealing condition, where a strongly localized state of charge carriers accompanied by an AF pseudogap at around the crossing points in the improper annealing condition has been changed to metallic- and SC states with the optimal annealing condition. In particular, the experimental observations of these single crystals in the proper annealing condition indicate clearly that the annealing and oxygen vacancy induce a sufficient change in the charge carrier density [16]. In this case, the doping concentration should be considered in conjunction with the annealing and oxygen nonstoichiometry. This actual charge carrier concentration has been used in building the new phase diagram [16–20], where the SC-state that coexists with AFSRO is extended over a wide electron doping range with a maximum value of $T_c$ that occurs at around the optimal doping $\delta \sim 0.15$, while the deduced AFLRO phase boundary does not extend into the SC dome [17–20]. This new phase diagram of electron-doped cuprate superconductors is strikingly analogous to the corresponding phase diagram in the hole-doped counterparts, and therefore reveals a possibility for the absence of the disparity between the phase diagrams of electron- and hole-doped cuprate superconductors.

*spfeng@bnu.edu.cn

With this new phase diagram, a critical question is whether the SC mechanism in the electron-doped side is the same as that in the hole-doped case.

The new phase diagram in the electron-doped cuprate superconductors is thus closely related to the actual electron doping concentration, while such an aspect should be reflected in the nature of the quasiparticle excitations resulting from the dressing of the electrons due to the electron interaction mediated by various bosonic excitations. An understanding of how the strong coupling of the electrons with various bosonic excitations affects the electronic structure is especially important to explain the astonishing phenomena, including the question of the pairing mechanism [21–23]. Very recently, the intrinsic EFS reconstruction and its evolution with electron doping in the new single crystals with the proper annealing condition were observed experimentally from angle-resolved photoemission spectroscopy (ARPES) measurements [17–20], where the characteristic features can be summarized as follows: (a) a quasiparticle peak is observed on the entire EFS without the signature of an AF pseudogap at around the crossing points; and (b) stronger quasiparticle scattering is observed in the antinodal region than in the nodal region, leading to the formation of the disconnected Fermi arcs centered around the nodal region. In the hole-doped case, the intrinsic features of the quasiparticle excitations, associated with the EFS reconstruction and characterized by the distinct depression in the electron density of states, reminiscent of the well-known peak-dip-hump (PDH) structure in the quasiparticle excitation spectrum, the kink in the quasiparticle dispersion, and the multiple nearly-degenerate electronic orders, have been observed experimentally by virtue of systematic studies using the scanning tunneling microscopy [24,25] and resonant X-ray scattering techniques [26–28], particularly the ARPES measurements [29–38]. On the other hand, although a few experimental results for the dispersion kinks along the nodal and antinodal directions, associated with the new phase diagram and the intrinsic EFS reconstruction, have been observed very recently in the electron-doped side with the proper annealing condition [20], to date the experimental data of the PDH structure are still lacking. Furthermore, to the best of our knowledge, these intrinsic properties of the quasiparticle excitations have also not been discussed starting from a SC theory so far. In this case, the crucial issue is to understand even from a theoretical analysis which intrinsic aspects of the quasiparticle excitations are universal to both electron- and hole-doped cuprate superconductors, and how they might depend on the specifics of the participating electron- or hole-like states.

In our previous works [39–43], the doping dependence of $T_c$ and the related dressing of the electrons in the hole-doped cuprate superconductors were investigated within the framework of kinetic-energy driven superconductivity, where we have shown that $T_c$ takes a domelike shape with the underdoped and overdoped regimes on each side of the optimal doping $\delta \sim 0.15$, where $T_c$ reaches its maximum, and then the main aspects of the quasiparticle excitations observed from the experiments, including the EFS reconstruction [44–48], the nature of the charge-order correlation [24–28], the striking PDH structure in the quasiparticle excitation spectrum [29–33], the dispersion kink [34–38], and the

remarkable ARPES autocorrelation and its connection with the quasiparticle scattering interference [48,49], are qualitatively reproduced. In particular, we have also shown that all these exotic features are a natural result of the strong electron correlation characterized by the strong electron interaction mediated by a strongly dispersive spin excitation. However, a comprehensive discussion of the electron-doped counterparts has not been given. We believe that if the coupling of the electrons with a strongly dispersive spin excitation is of the same nature both in the electron- and hole-doped cuprate superconductors, it should reveal itself in the nature of the quasiparticle excitation of the electron-doped cuprate superconductors as it does in the hole-doped counterparts. In this paper, we try to study the phase diagram and the related intrinsic properties of the quasiparticle excitations in electron-doped cuprate superconductors. We show explicitly that the maximal $T_c$ occurs around the optimal doping $\delta \sim 0.15$, and then decreases in both the underdoped and overdoped regimes. In particular, although the optimized $T_c$ in the electron-doped side is much smaller than that in the hole-doped case, the electron- and hole-doped cuprate superconductors rather resemble each other in the doping range of the SC dome, indicating an absence of the disparity between the phase diagrams of the electron- and hole-doped cuprate superconductors. Moreover, the characteristic features of the intrinsic EFS reconstruction, the PDH structure, and the dispersion kink in the electron-doped cuprate superconductors are a clear analogy to those obtained in the hole-doped counterparts. Our present results therefore also show that the essential physics is the same for both the electron- and hole-doped cuprate superconductors.

This paper is organized as follows. First, we present the basic formalism in Sec. II, where we express explicitly the single-particle diagonal and off-diagonal propagators (hence the single-particle spectral function) of the electron-doped cuprate superconductors based on the kinetic-energy driven superconductivity. We then discuss the doping dependence of $T_c$ in Sec. III, where a comparison of the phase diagrams between the electron- and hole-doped cuprate superconductors is made. In Sec. IV, we discuss the intrinsic aspects of the quasiparticle excitations, and we show that a sharp quasiparticle peak emerges on the entire EFS without an AF pseudogap at around the crossing points. Finally, we give a summary and discussions in Sec. V.

## II. FORMALISM

Both electron- and hole-doped cuprate superconductors have a layered crystal structure consisting of two-dimensional $CuO_2$ planes separated by insulating layers [1,2], and it is believed that the exotic features in these systems are closely related to the doped $CuO_2$ planes [5–8]. In this case, as originally emphasized by Anderson [3], the essential physics of the doped $CuO_2$ plane is properly captured by the $t$-$J$ model on a square lattice [50,51],

$$H = -t \sum_{l\hat{\eta}\sigma} C_{l\sigma}^\dagger C_{l+\hat{\eta}\sigma} + t' \sum_{l\hat{\tau}\sigma} C_{l\sigma}^\dagger C_{l+\hat{\tau}\sigma}$$
$$+ \mu \sum_{l\sigma} C_{l\sigma}^\dagger C_{l\sigma} + J \sum_{l\hat{\eta}} \mathbf{S}_l \cdot \mathbf{S}_{l+\hat{\eta}}, \quad (1)$$

where the summation is over all sites $l$, and for each $l$ over its nearest neighbor (NN) $\hat{\eta}$ or the next NN $\hat{\tau}$, the hopping integrals $t > 0$ and $t' > 0$ for the hole-doped case, while $t < 0$ and $t' < 0$ in the electron-doped side. In particular, the NN hopping $t$ in the $t$-$J$ model (1) has an electron-hole symmetry because the sign of $t$ can be absorbed by the change of the sign of the orbital on one sublattice. However, the electron-hole asymmetry can be properly accounted for by the next NN hopping $t'$ [52–54]. $C_{l\sigma}^{\dagger}$ and $C_{l\sigma}$ are the electron creation and annihilation operators, respectively, with spin $\sigma$ on site $l$, $\mathbf{S}_l$ is a localized spin operator, and $\mu$ is the chemical potential. The high complexity in the $t$-$J$ model (1) comes mainly from the electron local constraint, i.e., this $t$-$J$ model (1) is supplemented by a local constraint of no double electron occupancy in the hole-doped case: $\sum_{\sigma} C_{l\sigma}^{\dagger} C_{l\sigma} \leqslant 1$, while it acts on the space with no zero electron occupied sites in the electron-doped side: $\sum_{\sigma} C_{l\sigma}^{\dagger} C_{l\sigma} \geqslant 1$. However, for the electron doping, we can work in the hole representation via a particle-hole transformation $C_{l\sigma} \rightarrow f_{l-\sigma}^{\dagger}$, with $f_{l\sigma}^{\dagger}$ ($f_{l\sigma}$) that is the hole creation (annihilation) operator, and then the local constraint of no zero electron occupancy in the electron representation $\sum_{\sigma} C_{l\sigma}^{\dagger} C_{l\sigma} \geqslant 1$ is replaced by the local constraint of no double hole occupancy in the hole representation $\sum_{\sigma} f_{l\sigma}^{\dagger} f_{l\sigma} \leqslant 1$. In this case, the $t$-$J$ model (1) in both the electron doping and hole doping is always subject to an important on-site local constraint to avoid double occupancy, and the difference between electron doping and hole doping is expressed as the sign difference of the hopping integrals, as mentioned above. This local constraint of no double occupancy can be dealt with properly by the fermion-spin theory [55,56] based on the charge-spin separation, and in particular, the constrained hole operators $f_{l\uparrow}$ and $f_{l\downarrow}$ are decoupled as

$$f_{l\uparrow} = a_{l\uparrow}^{\dagger} S_l^{-}, \quad f_{l\downarrow} = a_{l\downarrow}^{\dagger} S_l^{+}, \tag{2}$$

where the spinful fermion operator $a_{l\sigma} = e^{-i\Phi_{l\sigma}} a_l$ describes the charge degree of freedom of the constrained hole together with some effects of spin configuration rearrangements due to the presence of the doped charge carrier itself, while the localized spin operator $S_l$ describes the spin degree of freedom of the constrained hole, and then the local constraint without double hole occupancy is satisfied in analytical calculations. Based on the $t$-$J$ model in the fermion-spin representation, the kinetic-energy driven SC mechanism has been established [56–58], where in the doped regime without an AFLRO, the coupling of the charge carriers and spin excitations directly from the kinetic energy provides the attractive interaction between the charge carriers in the particle-particle channel that pairs charge carriers together to form a $d$-wave charge-carrier pairing state. Then the electron pairs with $d$-wave symmetry originating from the $d$-wave charge-carrier pairing state are due to the charge-spin recombination [39], and their condensation reveals the SC ground state. The typical features of the kinetic-energy-driven SC mechanism can be summarized as follows: (a) the mechanism is purely electronic without phonons; (b) the mechanism indicates that the strong electron correlation favors superconductivity, since the main ingredient is identified in an electron pairing mechanism not involving the phonon, the external degree of freedom, but the internal spin degree of freedom of an electron; (c) the electron pairing state is controlled by both the electron pair gap and single-

particle coherence, which leads to the occurrence of maximal $T_c$ around the optimal doping, and then decreases in both the underdoped and the overdoped regimes; and (d) superconductivity coexists with the AFSRO correlation. Within the framework of this kinetic-energy-driven superconductivity, the ARPES autocorrelation and the line shape of the quasiparticle excitation spectrum in electron-doped cuprate superconductors have been studied recently [59]. Following these previous discussions [59], the single-particle diagonal and off-diagonal propagators $G(\mathbf{k}, \omega)$ and $\Im^{\dagger}(\mathbf{k}, \omega)$ of the electron-doped cuprate superconductors can be obtained explicitly as

$$G(\mathbf{k}, \omega) = \frac{1}{\omega - \varepsilon_{\mathbf{k}} - \Sigma_{\text{tot}}(\mathbf{k}, \omega)}, \tag{3a}$$

$$\Im^{\dagger}(\mathbf{k}, \omega) = \frac{L_{\mathbf{k}}(\omega)}{\omega - \varepsilon_{\mathbf{k}} - \Sigma_{\text{tot}}(\mathbf{k}, \omega)}, \tag{3b}$$

where $\varepsilon_{\mathbf{k}} = 4t\gamma_{\mathbf{k}} - 4t'\gamma_{\mathbf{k}}' - \mu$ is the single-electron band energy, with $\gamma_{\mathbf{k}} = (\cos k_x + \cos k_y)/2$ and $\gamma_{\mathbf{k}}' = \cos k_x \cos k_y$, $L_{\mathbf{k}}(\omega) = -\Sigma_{pp}(\mathbf{k}, \omega)/[\omega + \varepsilon_{\mathbf{k}} + \Sigma_{ph}(\mathbf{k}, -\omega)]$, while the total self-energy $\Sigma_{\text{tot}}(\mathbf{k}, \omega)$ is a combination of the normal self-energy $\Sigma_{ph}(\mathbf{k}, \omega)$ in the particle-hole channel and the anomalous self-energy $\Sigma_{pp}(\mathbf{k}, \omega)$ in the particle-particle channel, and it is given explicitly by

$$\Sigma_{\text{tot}}(\mathbf{k}, \omega) = \Sigma_{ph}(\mathbf{k}, \omega) + \frac{|\Sigma_{pp}(\mathbf{k}, \omega)|^2}{\omega + \varepsilon_{\mathbf{k}} + \Sigma_{ph}(\mathbf{k}, -\omega)}. \tag{4}$$

In the kinetic-energy-driven SC mechanism, both the normal and anomalous self-energies $\Sigma_{ph}(\mathbf{k}, \omega)$ and $\Sigma_{pp}(\mathbf{k}, \omega)$ quantify the interaction between electrons mediated by a strongly dispersive spin excitation, and they have been given explicitly in Ref. [59], where the sharp peak visible for temperature $T \rightarrow 0$ in the normal (anomalous) self-energy is actually a $\delta$-function broadened by a small damping used in the numerical calculation at a finite lattice. The calculation in this paper for the normal (anomalous) self-energy is performed numerically on a $160 \times 160$ lattice in momentum space, with the infinitesimal $i0_+ \rightarrow i\Gamma$ replaced by a small damping $\Gamma = 0.1J$.

The result in Eq. (3) also shows that the basic Eliashberg formalism [60] with the $d$-wave type SC gap is still valid, although the pairing mechanism is driven by the kinetic energy by the exchange of spin excitations. The single-particle spectral function $A(\mathbf{k}, \omega)$ is related directly to the imaginary part of the single-particle diagonal propagator in Eq. (3a) as [5–7]

$$A(\mathbf{k}, \omega) = \frac{-2 \operatorname{Im} \Sigma_{\text{tot}}(\mathbf{k}, \omega)}{[\omega - \varepsilon_{\mathbf{k}} - \operatorname{Re} \Sigma_{\text{tot}}(\mathbf{k}, \omega)]^2 + [\operatorname{Im} \Sigma_{\text{tot}}(\mathbf{k}, \omega)]^2}, \tag{5}$$

and then the quasiparticle excitation spectrum measured by ARPES experiments is proportional to this single-particle spectral function (5), where $\operatorname{Re} \Sigma_{\text{tot}}(\mathbf{k}, \omega)$ and $\operatorname{Im} \Sigma_{\text{tot}}(\mathbf{k}, \omega)$ are the real and imaginary parts of the total self-energy $\Sigma_{\text{tot}}(\mathbf{k}, \omega)$, respectively. In particular, the real part of the total self-energy offsets the single-electron band energy $\varepsilon_{\mathbf{k}}$, while the imaginary part of the total self-energy is identified as the quasiparticle scattering rate,

$$\Gamma(\mathbf{k}, \omega) = \operatorname{Im} \Sigma_{\text{tot}}(\mathbf{k}, \omega), \tag{6}$$

which broadens the spectral peak in the ARPES spectrum, and therefore governs the lifetime of the quasiparticle [5–7].
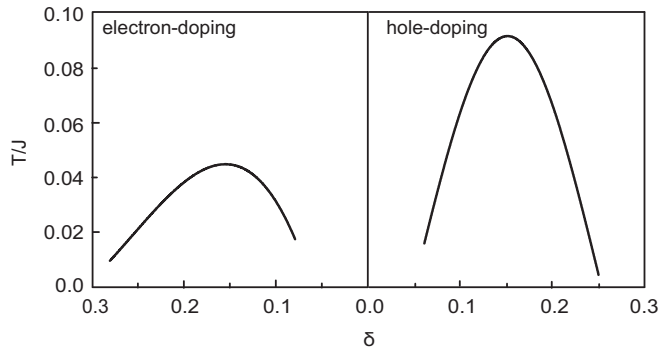
FIG. 1. Left panel: the doping dependence of the superconducting transition-temperature in the electron-doped side for $t/J = -2.5$ and $t'/t = 0.3$. Right panel: the corresponding result in the hole-doped case for $t/J = 2.5$ and $t'/t = 0.3$ taken from Ref. [39].

This is why one can obtain the information about the total self-energy from ARPES experiments by analyzing the energy and momentum distribution data.

## III. PHASE DIAGRAM

The understanding of the phase diagram of cuprate superconductors has been one of the central issues since its original discovery in 1986 [1,2] through to the present day. Within the framework of the kinetic-energy-driven superconductivity [56–58], the evolution of $T_c$ with the hole doping in hole-doped cuprate superconductors has been obtained in our early studies [39,58] in terms of the self-consistent calculation at the condition of the SC gap $\bar{\Delta} = 0$, where $T_c$ has a domelike shape doping dependence with the maximum $T_c$ that occurs around the optimal hole doping $\delta \sim 0.15$, in good agreement with the experimental results observed on the hole-doped cuprate superconductors [61]. Following these early studies for the hole-doped case, we have also performed a self-consistent calculation for the doping dependence of $T_c$ in the electron-doped side, and the result of $T_c$ as a function of the electron doping for parameters $t/J = -2.5$ and $t'/t = 0.3$ is plotted in the left panel of Fig. 1. To compare the present result of the electron-doped cuprate superconductors with that of their hole-doped counterparts, the corresponding result [39] of the doping dependence of $T_c$ in the hole-doped case for parameters $t/J = 2.5$ and $t'/t = 0.3$ is also shown in the right panel of Fig. 1. One can immediately see from the results in Fig. 1 that the doping range of the SC dome in the electron-doped side is very similar to that in the hole-doped case, where with the increase of doping, $T_c$ is raised gradually in the underdoped regime, and it reaches the maximum around the optimal doping $\delta \sim 0.15$; however, the optimized $T_c$ in the electron-doped side is much lower than that in the hole-doped case. With a further increase of doping, $T_c$ then decreases monotonically in the overdoped regime, and finally superconductivity disappears in the heavily overdoped regime. Apart from this obvious similarity of the doping ranges of the SC domes in the electron- and hole-doped cuprate superconductors, the other typical features in Fig. 1 can also be summarized as follows: (a) there is no disparity between the phase diagrams of the electron- and hole-doped cuprate superconductors;
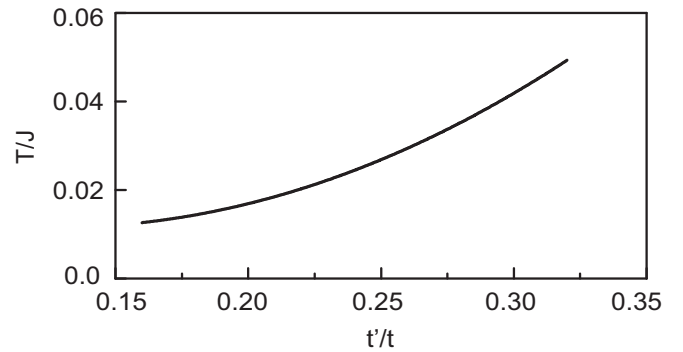


FIG. 2. The maximal superconducting transition-temperature as a function of $t'$ at the electron doping $\delta = 0.15$ for $t/J = -2.5$.

(b) superconductivity coexists with the AFSRO correlation; and (c) as evidence of the electron-hole asymmetry, $T_c$ in the hole-doped case is much higher than that in the electron-doped side. This electron doping dependence of $T_c$ in the left panel of Fig. 1 and the related typical features are well consistent with the true phase diagram observed recently on $Pr_{1-x}LaCe_xCuO_{4-\delta}$ under the proper annealing condition [18,19] and the corresponding $\mu$SR experimental results [62]. The good agreement between the present theoretical result of the phase diagram in Fig. 1 and experimental observations also shows the existence of a common SC mechanism for both electron- and hole-doped cuprate superconductors.

However, it should be noted that in both electron- and hole-doped cuprate superconductors, the values of $t$, $t'$, and $J$ are believed to vary somewhat from compound to compound [52–54,63–71], and then some differences were observed experimentally among the different families, such as the significant variation in the maximal $T_c$ at optimal doping [5–8]. In particular, it has been shown experimentally and theoretically that maximal $T_c$ (and then the shape of the SC dome) for different families of hole-doped cuprate superconductors [69–71] is strongly correlated with $t'$. In this case, we have made a series of calculations for maximal $T_c$ at optimal doping with different values of $t'$ in the electron-doped cuprate superconductors, and the results show that maximal $T_c$ is also correlated with $t'$. To see this correlation more clearly, we plot maximal $T_c$ as a function of $t'$ at the electron doping $\delta = 0.15$ for $t/J = -2.5$ in Fig. 2, where in a reasonably estimative range [52–54,63–68] of the parameter $t'$, maximal $T_c$ is enhanced by $t'$, i.e., maximal $T_c$ increases smoothly with the increase of $t'$. This anticipated result is also well consistent with the corresponding experimental data [69] of the hole-doped counterparts, and the numerical simulations [70,71] in the same range of the parameter $t'$, where the enhancement of $T_c$ by $t'$ has been observed experimentally and confirmed by numerical simulations.

## IV. EXOTIC FEATURES OF THE DRESSING OF ELECTRONS

The dressing of the electrons due to the strong coupling of the electrons with various bosonic excitations leads to a rich variety of phenomena. However, with the new phase diagram in Fig. 1, the immediate problem becomes determining which
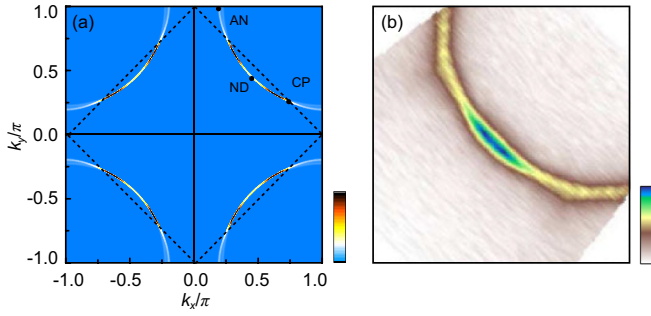
FIG. 3. (a) The electron Fermi surface map at the electron doping $\delta = 0.15$ with $T = 0.002J$ for $t/J = -2.5$ and $t'/t = 0.3$, where the dotted line represents the antiferromagnetic Brillouin zone boundary, while AN, CP, and ND denote antinode, crossing point, and node, respectively. (b) The experimental result of the electron Fermi surface for $Pr_{1-x}LaCe_xCuO_{4-\delta}$ under the proper annealing at around the electron doping $\delta = 0.15$ taken from Ref. [18].

of these astonishing phenomena are universal to both the electron- and hole-doped cuprate superconductors, and how these astonishing phenomena depend on the specifics of the participating electron- or holelike states.

### A. Intrinsic electron Fermi surface reconstruction

In ARPES experiments [5–7], the weight of the ARPES spectrum at zero energy is used to map out EFS. In other words, EFS is determined by the single-particle spectral function $A(\mathbf{k}, \omega = 0)$ in Eq. (5) at zero energy to map out the locus of the maximum in the spectral weight of $A(\mathbf{k}, \omega = 0)$. For an understanding of the essential physics of an interacting system, a study of the nature of EFS is a starting point [72]. This follows from the fact that the EFS topology is a fundamental ground-state property, and it influences directly the low-energy transport properties. In particular, the shape of EFS in cuprate superconductors has been central to addressing the strong electron correlation effect and multiple nearly degenerate electronic orders [24–28,73,74]. In this case, we first characterize the EFS topology. In the case without considering the electron interaction, a large EFS is characterized as a closed contour of the gapless quasiparticle excitations in momentum space, where the peaks of the quasiparticle excitation spectrum with the same weight distribute uniformly along with the EFS contour, and then the quasiparticle lifetime is infinitely long on this EFS contour. However, in the presence of the strong interaction of the electrons with a strongly dispersive spin excitation, which is manifested by the energy and momentum dependence of the total self-energy $\Sigma_{tot}(\mathbf{k}, \omega)$, the closed EFS contour is broken up into the disconnected Fermi arcs. To see this EFS reconstruction more clearly, we plot the underlying EFS map in the $[k_x, k_y]$ plane at the electron doping $\delta = 0.15$ with $T = 0.002J$ for $t/J = -2.5$ and $t'/t = 0.3$ in Fig. 3(a). For comparison, the experimental result [18] obtained from the ARPES measurement on $Pr_{1-x}LaCe_xCuO_{4-\delta}$ under proper annealing at around electron doping $\delta = 0.15$ is also shown in Fig. 3(b). In qualitative analogy to the hole-doped counterparts [39,40], EFS has been reconstructed due to the strong redistribution of the spectral weight, where there are two typical regions: (a) the antinodal region, where the

result shows a heavy suppression of the spectral weight, causing EFS to be invisible around the antinodal region, and the AF pseudogap at around the crossing points is totally absent; and (b) the nodal region, where the result indicates a modest reduction of the spectral weight, and then EFS is clearly visible as a reminiscence of the EFS contour in the case without considering the electron interaction forming the Fermi arcs centered around the nodal region. However, the dressing from the quasiparticle scattering further moves the spectral weight from the Fermi arcs to the tips of the Fermi arcs, which leads to the fact that although a quasiparticle peak emerges in the entire EFS, the spectral weight exhibits the largest value at around the tips of the Fermi arcs. This EFS reconstruction is also qualitatively consistent with recent experimental observations of electron-doped cuprate superconductors [17–20], whereupon proper annealing, (a) the weight of the ARPES spectrum around the antinodal region is suppressed, and then EFS is truncated to form the Fermi arcs located around the nodal region; and (b) the AF pseudogap is closed on the whole EFS, and then the quasiparticle peak is observed on the whole EFS. Moreover, as in the hole-doped case [42,48,49], these tips of the Fermi arcs linked up by the scattering wave vectors $\mathbf{q}_i$ in the electron-doped side also can construct an *octet* scattering model [59], and then different ordered electronic states determined by the quasiparticle scattering processes with the corresponding scattering wave vectors $\mathbf{q}_i$ are therefore driven by this intrinsic EFS instability. This is also why an exotic feature in the electron-doped cuprate superconductor is the coexistence and competition between different ordered electronic states and superconductivity [8,73,74]. In particular, it has been shown that the charge-order wave vector $\mathbf{q}_1 = \mathbf{Q}_{co}$ connecting the straight tips of the Fermi arcs smoothly *increases* with the increase of the electron doping [75], which is consistent with the experimental results [74]. However, this is unlike the case in the hole-doped counterparts [27,28,40], where the charge-order wave vector smoothly *decreases* with the increase of the hole doping, which is more evidence of the electron-hole asymmetry. Furthermore, we have also studied the doping dependence of the EFS reconstruction, and the results show that the EFS reconstruction can persist into the overdoped regime, also in agreement with the experimental observations [17–20].

The physical origin of the EFS reconstruction in the electron-doped side is the same as that in the hole-doped case [40], and it can also be attributed to the highly anisotropic momentum dependence of the quasiparticle scattering rate (6). The EFS contour in momentum space is determined directly by the poles of the single-particle diagonal propagator (3a) at zero energy: $\varepsilon_{\mathbf{k}} + \mathrm{Re}\Sigma_{tot}(\mathbf{k}, 0) = 0$, and then the spectral weight of the single-particle spectral function $A(\mathbf{k}, 0)$ in Eq. (5) at EFS is governed by the inverse of the quasiparticle scattering rate $1/\Gamma(\mathbf{k}, 0)$. To reveal this highly anisotropic $\Gamma(\mathbf{k}, 0)$ in momentum space clearly, we plot the angular dependence of $\Gamma(\mathbf{k}_F, 0)$ along EFS from the antinode to the node at $\delta = 0.15$ with $T = 0.002J$ for $t/J = -2.5$ and $t'/t = 0.3$ in Fig. 4 in comparison with the corresponding ARPES result [17] observed on $Pr_{1.3-x}La_{0.7}Ce_xCuO_4$ under the proper annealing condition (inset). Apparently, the main feature of the quasiparticle scattering rate along EFS observed from the ARPES experiment [17] is qualitatively reproduced, where
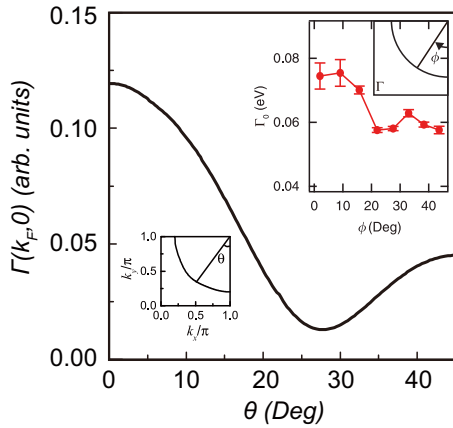
FIG. 4. The angular dependence of the quasiparticle scattering rate along $\mathbf{k}_F$ from the antinode to the node at $\delta = 0.15$ with $T = 0.002J$ for $t/J = -2.5$ and $t'/t = 0.3$. Inset: the corresponding experimental data of $Pr_{1.3-x}La_{0.7}Ce_xCuO_4$ under the proper annealing condition taken from Ref. [17].
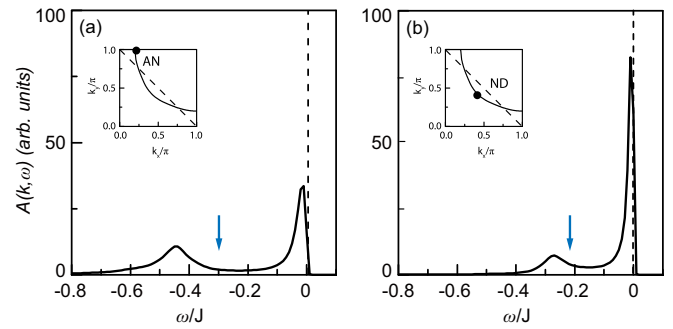


FIG. 5. The quasiparticle excitation spectrum as a function of energy at (a) the antinode and (b) the node in $\delta = 0.15$ with $T = 0.002J$ for $t/J = -2.5$ and $t'/t = 0.3$, where the blue arrow indicates the position of the dip, while AN and ND in the insets denote antinode and node, respectively.

the quasiparticle scattering rate increases as the momentum approaches the antinode, and then the strongest scattering emerges at the antinode, leading to a heavy suppression of the spectral weight around the antinode. Moreover, the weak quasiparticle scattering occurs around the nodal region, and then the formation of the Fermi arcs is due to a modest reduction of the spectral weight around the nodal region. This strong redistribution of the spectral weight on EFS therefore induces the EFS reconstruction or instability. It is very interesting to note that a similar angular dependence of the quasiparticle scattering rate was also observed experimentally in the hole-doped case [76], indicating a common quasiparticle scattering mechanism both in the hole- and electron-doped cuprate superconductors.

However, as seen by a comparison with the experimental data [17], there is also a substantial difference between theory and experiment, namely the weakest quasiparticle scattering occurs at the crossing points in experiment [17], while the calculation in the present parameters $t/J = -2.5$ and $t'/t = 0.3$ anticipates it at the tips of the Fermi arcs. In the electron-doped cuprate superconductors, (a) as we have mentioned above in Sec. III, the values of $t$, $t'$, and $J$ are different between different families [63–68]; (b) however, the positions of the tips of the Fermi arcs are strongly dependent on the curvature of EFS, while this curvature [63–68] is dominated by the next NN hopping $t'$. In other words, the difference in $t'$ among the electron-doped cuprate superconductors [63–68] leads to the difference of the positions of the tips of the Fermi arcs. In this case, we have also made a series of calculations for the different value of $t'$, and we found that the positions of the tips of the Fermi arcs can be located exactly on the corresponding positions of the crossing points by the proper choice or adjustment of the parameter $t'$.

### B. Peak-dip-hump structure

The dressing of the electrons affects the quasiparticle excitation spectrum and the momentum and energy dependence of the quasiparticle scattering rate, which can be obtained,

respectively, from the energy distribution curves and the widths of the corresponding peaks in ARPES experiments [5–7]. In the hole-doped cuprate superconductors, a hallmark of the spectral line shape of the ARPES spectrum is the well-known PDH structure [29–33], which is closely associated with the EFS reconstruction, and now has been identified experimentally along the entire EFS. Since the strong coupling of the electrons with bosonic excitations has been observed experimentally in whole families of hole-doped cuprate superconductors within a wide hole-doping range, it is thus believed that the strong coupling of electrons with bosonic excitations gives rise to the PDH structure [29–33]. In particular, we [40,41] have shown based on the kinetic-energy-driven SC mechanism that this strong coupling of the electrons with bosonic excitations can be identified as the strong electron coupling to a strongly dispersive spin excitation. In this subsection, we discuss the spectral line shape in the quasiparticle excitation spectrum of the electron-doped cuprate superconductors. We have performed a calculation for the single-particle spectral function (5), and the results of $A(\mathbf{k}, \omega)$ as a function of energy at (a) the antinode and (b) the node for $\delta = 0.15$ with $T = 0.002J$ for $t/J = -2.5$ and $t'/t = 0.3$ are plotted in Fig. 5, where we find that the main features of the PDH structure in the electron-doped side are in striking similarity with those obtained in the hole-doped case [29–33,40,41]. In particular, the position of the dip in the PDH structure is shifted to lower energy when one moves the momentum from the antinode to the node, while the coupling strength of the electrons with a strongly dispersive spin excitation appears to be weaker at around the nodal region than at around the antinodal region. Moreover, the results in Fig. 5 also show that the PDH structure is an intrinsic feature of the quasiparticle excitation spectrum in the electron-doped cuprate superconductors, and is found to be present all around EFS. Although the experimental data of the PDH structure in the quasiparticle excitation spectrum of the electron-doped cuprate superconductors under the proper annealing condition are still lacking to date, a similar PDH structure has been observed experimentally on the electron-doped cuprate superconductors under the improper annealing condition [8–12], while our present results in Fig. 5 are also
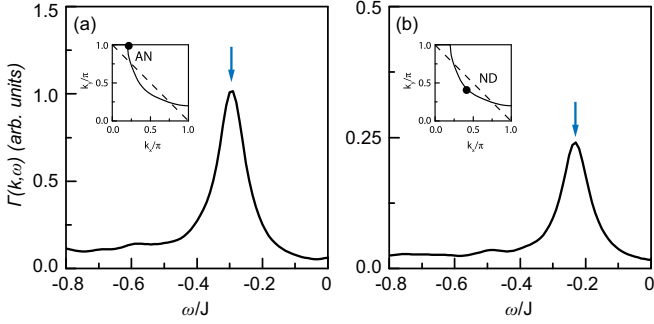
FIG. 6. The quasiparticle scattering rate at (a) the antinode and (b) the node as a function of energy in $\delta = 0.15$ with $T = 0.002J$ for $t/J = -2.5$ and $t'/t = 0.3$, where the blue arrow indicates the position of the peak, and AN and ND in the insets denote antinode and node, respectively.

qualitatively consistent with these experimental observations [8–12].

The mechanism of the PDH structure in the quasiparticle excitation spectrum of electron-doped cuprate superconductors is also the same as in their hole-doped counterparts [33,40,41], and it is directly associated with the emergence of the corresponding sharp peak in the quasiparticle scattering rate. Following the single-particle spectral function in Eq. (5), the position of the peak in the momentum distribution curve, plotted as a function of energy in Fig. 5, is determined self-consistently by the quasiparticle dispersion

$$\bar{E}_{\mathbf{k}} = \varepsilon_{\mathbf{k}} + \text{Re}\,\Sigma_{\text{tot}}(\mathbf{k}, \bar{E}_{\mathbf{k}}), \qquad (7)$$

while the weight of the peak (then the lifetime of the quasiparticle excitation) is dominated by the inverse of the quasiparticle scattering rate $\Gamma(\mathbf{k}, \omega)$. In this case, the appearance of the dip in the PDH structure of the quasiparticle excitation spectrum along EFS is closely related to the emergence of the corresponding sharp peak in $\Gamma(\mathbf{k}, \omega)$. To see this point more clearly, we plot $\Gamma(\mathbf{k}, \omega)$ as a function of energy at (a) the antinode and (b) the node for $\delta = 0.15$ with $T = 0.002J$ for $t/J = -2.5$ and $t'/t = 0.3$ in Fig. 6, where the sharp peaks emerge at the antinode and node, respectively. More specifically, we find that the position of the peak in $\Gamma(\mathbf{k}, \omega)$ at the antinode (node) in Fig. 6 corresponds exactly to the position of the dip in the PDH structure in the quasiparticle excitation spectrum at the antinode (node) shown in Fig. 5, and then the spectral weight at around the dip is suppressed heavily by the corresponding sharp peak in $\Gamma(\mathbf{k}, \omega)$, which leads to forming the PDH structure in the quasiparticle excitation spectrum. In other words, the striking PDH structure in the quasiparticle excitation spectrum shown in Fig. 5 is caused directly by the emergence of the sharp peak in $\Gamma(\mathbf{k}, \omega)$ shown in Fig. 6. Furthermore, we have also discussed the spectral line shape in the electron-doped cuprate superconductors in the normal state, and we found a sharp peak in $\Gamma(\mathbf{k}, \omega)$ that can persist into the normal state, indicating that the PDH structure is totally unrelated to superconductivity, as is the PDH structure in the hole-doped counterparts [29–33].

## C. Dispersion kink

The strong coupling of the electrons and various bosonic excitations in cuprate superconductors manifested itself as a slope change (or a kink) in the quasiparticle dispersion [5–7]. In the hole-doped cuprate superconductors, the quasiparticle dispersion displays a kink around EFS [34–38], with the energy range 50–80 meV at which the kink appears. In spite of the extensive studies, the controversy still exists as to what bosonic mode causes the dispersion kink. In recent studies for the hole-doped case [43], we have shown within the framework of the kinetic-energy-driven superconductivity that the quasiparticle dispersion is affected by a strongly dispersive spin excitation, and then the dispersion kink associated with the dressing of the electrons is electronic in nature. On the electron-doped side, although the experimental results of the PDH structure in the quasiparticle excitation spectrum under the proper annealing condition are still lacking to date, as we have mentioned above in Sec. I, the dispersion kinks in the electron-doped cuprate superconductor $\text{Pr}_{1.3-x}\text{La}_{0.7}\text{Ce}_x\text{CuO}_4$ under the proper annealing condition along the nodal and antinodal directions have been detected very recently from the ARPES spectra [20], where the *bare* band structure [20,77] has been well fitted in terms of the single-band tight-binding model with $t'/t = 0.15$–$0.19$. In this subsection, we discuss the nature of the dispersion kink in the electron-doped cuprate superconductors, and we adopt the parameters $t/J = -2.5$ and $t'/t = 0.16$ in the $t$-$J$ model (1) for a quantitative or semiquantitative comparison between theory and experiment.

In Fig. 7, we plot the intensity map of the single-particle spectral function as a function of binding energy along (a) the nodal cut and (b) the antinodal cut at $\delta = 0.15$ with $T = 0.002J$ for $t/J = -2.5$ and $t'/t = 0.16$ in the upper panel. In the lower panel, we plot the corresponding quasiparticle dispersions along (c) the nodal cut and (d) the antinodal cut extracted from the positions of the lowest-energy quasiparticle excitation peaks in (a) and (b), respectively. The arrow in Fig. 7 marks the kink where the linear quasiparticle dispersion is separated as the low-energy and high-energy ranges with different slopes. It is especially interesting to note that these results of the dispersion kink in the electron-doped cuprate superconductors shown in Fig. 7 are quite similar to those obtained in the hole-doped counterparts [34–38,43]. In particular, with a reasonably estimative value of $J \sim 100$ meV, the quasiparticle dispersion deviates from the low-energy linear dispersion at around the kink energy $\omega_{\text{kink}} \sim 0.79J = 79$ meV along the nodal cut, while this kink energy occurs at around $\omega_{\text{kink}} \sim 0.40J = 40$ meV along the antinodal cut, which are semiquantitatively consistent with the corresponding results [20] observed on the electron-doped cuprate superconductor $\text{Pr}_{1.3-x}\text{La}_{0.7}\text{Ce}_x\text{CuO}_4$ under the proper annealing condition along the nodal and antinodal directions, respectively. The results in Fig. 7 also indicate that although the kink in the quasiparticle dispersion is present all around EFS, the kink energy decreases when the cut moves from the nodal region to the antinodal region. Moreover, it should be noted that the coupling of the electrons with bosonic excitations has also been observed early in all the electron-doped cuprate superconductors under the improper annealing condition [78–81], where the quasiparticle dispersions present the kinks at around
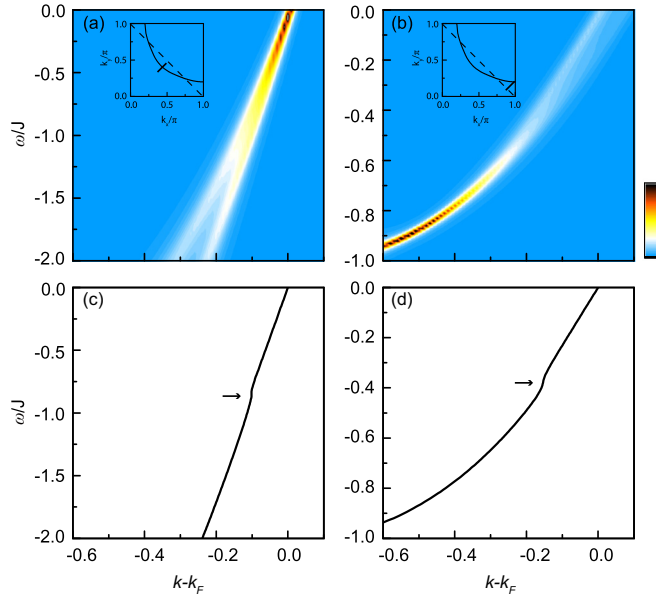
FIG. 7. Upper panel: the intensity maps of the electron spectral function as a function of binding energy along (a) the nodal cut and (b) the antinodal cut at $\delta = 0.15$ with $T = 0.002J$ for $t/J = -2.5$ and $t'/t = 0.16$, where the insets show the respective locations of the two cuts in the Brillouin zone relative to the electron Fermi surface. Lower panel: the quasiparticle dispersions along (c) the nodal cut and (d) the antinodal cut extracted from the positions of the lowest-energy quasiparticle excitation peaks in (a) and (b), respectively, where the arrow indicates the kink position.
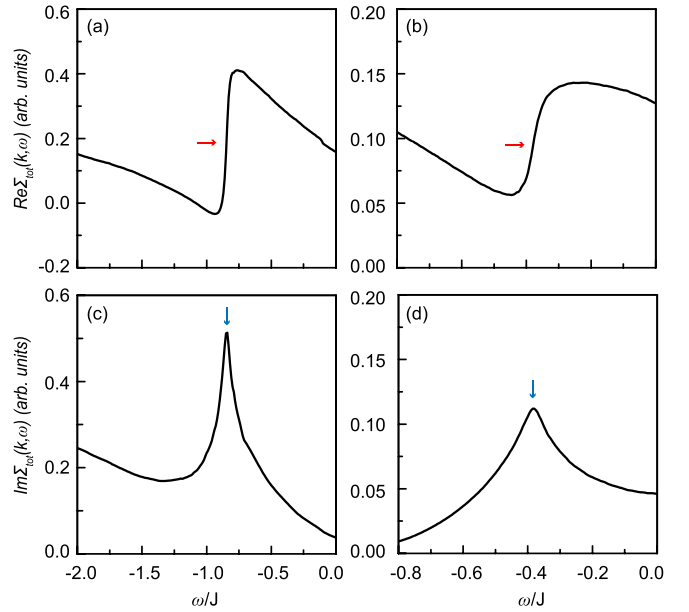


FIG. 8. Upper panel: the real part of the total self-energy as a function of binding energy along (a) the nodal dispersion and (b) the antinodal dispersion at $\delta = 0.15$ with $T = 0.002J$ for $t/J = -2.5$ and $t'/t = 0.16$, where the red arrow indicates the inflection point. Lower panel: the quasiparticle scattering rate as a function of binding energy along (c) the nodal dispersion and (d) the antinodal dispersion, where the blue arrow denotes the peak position.

50–70 meV along both the antinodal and nodal cuts, which are also semiquantitatively consistent with our present results in Fig. 7.

A natural and important question is, which bosonic mode causes the dispersion kink in the electron-doped cuprate superconductors? Within the framework of the kinetic-energy-driven superconductivity, the dispersion kink in the electron-doped cuprate superconductors arises from the strong coupling between the electrons and a strongly dispersive spin excitation. This follows the fact that from the quasiparticle dispersion in Eq. (7), the dispersion kink shown in Fig. 7 does not originate from the single-electron band energy $\varepsilon_{\mathbf{k}}$, but it is due to the slope change in the real part of the total self-energy $\mathrm{Re}\,\Sigma_{\mathrm{tot}}(\mathbf{k}, \omega)$, while the drop seen around the kink is directly associated with the corresponding peak in the quasiparticle scattering rate $\Gamma(\mathbf{k}, \omega)$ in Eq. (6) (then the imaginary part of the total self-energy). To further explore how the total self-energy generates the dispersion kink, we plot the real part of the total self-energy $\mathrm{Re}\,\Sigma_{\mathrm{tot}}(\mathbf{k}, \omega)$ as a function of binding energy along (a) the nodal dispersion and (b) the antinodal dispersion as shown in Figs. 7(c) and 7(d), respectively, at $\delta = 0.15$ with $T = 0.002J$ for $t/J = -2.5$ and $t'/t = 0.16$ in the upper panel of Fig. 8, where the red arrow indicates the inflection point (and then the point of the slope change in the quasiparticle dispersion). In the lower panel, we plot the corresponding quasiparticle scattering rate $\Gamma(\mathbf{k}, \omega)$ as a function of binding energy along (c) the nodal dispersion and (d) the antinodal dispersion, where the blue arrow denotes the peak position (and then the point of the intensity

depletion in the quasiparticle dispersion). It is obvious that a well-pronounced peak in $\Gamma(\mathbf{k}, \omega)$ is clearly visible with a corresponding inflection point in $\mathrm{Re}\,\Sigma_{\mathrm{tot}}(\mathbf{k}, \omega)$ that appears at the exactly same energy in $\Gamma(\mathbf{k}, \omega)$. This sharp peak in $\Gamma(\mathbf{k}, \omega)$ suppresses heavily the spectral weight at around the inflection point. More importantly, we find that the position of the dispersion kink in Fig. 7 matches exactly the position of the inflection point in $\mathrm{Re}\,\Sigma_{\mathrm{tot}}(\mathbf{k}, \omega)$ [and then the position of the peak in $\Gamma(\mathbf{k}, \omega)$] in Fig. 8. In other words, the emergence of the dispersion kink is determined by both the inflection point in $\mathrm{Re}\,\Sigma_{\mathrm{tot}}(\mathbf{k}, \omega)$ and the well-pronounced peak in $\Gamma(\mathbf{k}, \omega)$. This is why the dispersion kink marks the crossover between two different slopes, while the weak spectral intensity appears always at around the kink position [78–81].

### D. Peak structure in self-energy

In ARPES experiments [5–7], the energy distribution curves are observed when the photoemission intensity is measured at constant momentum, while the momentum distribution curves are observed when the photoemission intensity is measured at constant energy. The information of the energy and momentum dependence of the electron self-energy can then be extracted in terms of the single-particle spectral function (5) by analyzing the spectral intensity of the energy and momentum distribution curves. However, as shown in the single-particle spectral function (5), only the total self-energy can be extracted directly from ARPES experiments [5–7]. In particular, for our exploration of the strongly dispersive spin excitation coupling in the kinetic-energy-driven SC mechanism that is how the normal and anomalous self-energy effects

compete in the SC-state. It is thus crucial to extract the normal and the anomalous self-energies separately. This also follows a basic fact that in the kinetic-energy-driven superconductivity [39,56–58], the SC-state is controlled by both the electron pair gap and single-particle coherence, where the single-particle coherence is dominated by the normal self-energy $\Sigma_{ph}(\mathbf{k}, \omega)$, and therefore antagonizes superconductivity, while the energy- and momentum-dependent electron pair gap is determined completely by the anomalous self-energy $\Sigma_{pp}(\mathbf{k}, \omega)$, and therefore corresponds to the energy for breaking an electron pair. In this case, if both the normal and anomalous self-energies are deduced from the experimental data, we can examine the microscopic theory of the kinetic-energy-driven superconductivity and understand the essential physics of cuprate superconductors.

In the hole-doped cuprate superconductors, the machine-learning technique has been applied recently to deduce both the normal and anomalous self-energies from the experimental data of the ARPES spectra observed in $Bi_2Sr_2CaCu_2O_{8+\delta}$ at the optimum doping and $Bi_2Sr_2CuO_{6+\delta}$ in the underdoped regime [82], and the deduced results show clearly that both the normal and anomalous self-energies exhibit sharp low-energy peak structures. Moreover, these machine-learning "experimental" results confirm that the peak in the anomalous self-energy makes a dominant contribution to the SC gap, and thus they provide decisive testimony for the origin of superconductivity [82]. In very recent studies [83], we made a comparison of these deduced normal and anomalous self-energies in Ref. [82] with those obtained based on the kinetic-energy-driven SC mechanism, and then we showed explicitly that the interaction between electrons by the exchange of spin excitations generates sharp low-energy peak structures both in the normal and anomalous self-energies, in striking agreement with the corresponding results in the normal and anomalous self-energies deduced via machine learning "experiments" [82]. In this subsection, we analyze the normal and anomalous self-energies in the electron-doped cuprate superconductors, and then we compare these normal and anomalous self-energies with those obtained in the hole-doped counterparts [82,83].

In Fig. 9, we plot (a) the real (blue line) and imaginary (red line) parts of the normal self-energy, and (b) the real (blue line) and imaginary (red line) parts of the anomalous self-energy at the antinode as a function of energy in the electron doping $\delta = 0.15$ with $T = 0.002J$ for $t/J = -2.5$ and $t'/t = 0.3$. For a better comparison, the corresponding results [83] of (c) the real and imaginary parts of the normal self-energy, and (d) the real and imaginary parts of the anomalous self-energy at the antinode as a function of energy in the *hole* doping $\delta = 0.15$ with $T = 0.002J$ for $t/J = 2.5$ and $t'/t = 0.3$, are also shown in Fig. 9. Surprisingly, both the normal and anomalous self-energies in the electron-doped cuprate superconductors also exhibit sharp low-energy peak-structures. More specifically, the main features of these low-energy peak structures are in stark similarity with the corresponding low-energy peak structures in the normal and anomalous self-energies of the hole-doped cuprate counterparts obtained based on the kinetic-energy-driven superconductivity [83], and deduced from the ARPES spectra via machine learning [82]. This is why the absence of the disparity between
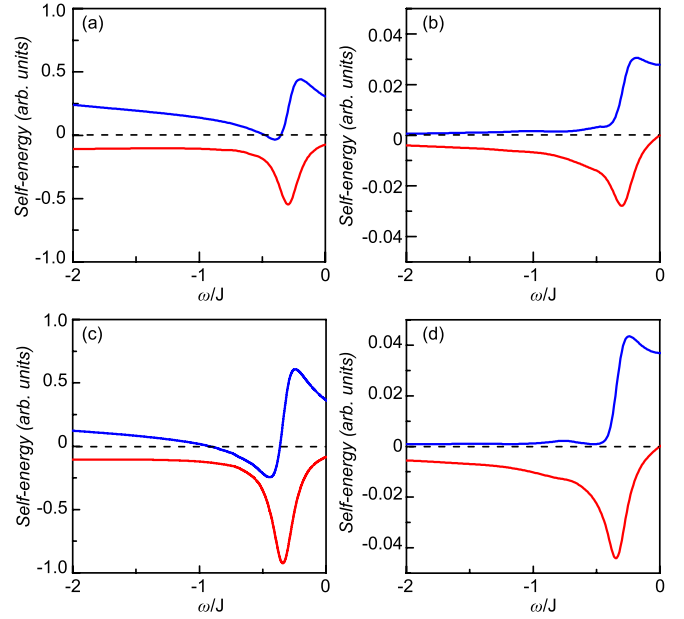


FIG. 9. (a) The real (blue line) and imaginary (red line) parts of the normal self-energy, and (b) the real (blue line) and imaginary (red line) parts of the anomalous self-energy at the antinode as a function of energy in the electron doping $\delta = 0.15$ with $T = 0.002J$ for $t/J = -2.5$ and $t'/t = 0.3$. The corresponding results of (c) the real and imaginary parts of the normal self-energy and (d) the real and imaginary parts of the anomalous self-energy of the hole-doped cuprate superconductors at the antinode as a function of energy in the hole doping $\delta = 0.15$ with $T = 0.002J$ for $t/J = 2.5$ and $t'/t = 0.3$ taken from Ref. [83].

the phase diagrams of the electron- and hole-doped cuprate superconductors can be observed experimentally [18–20]. In the SC-state, the pairing force and electron pair order parameter have been incorporated into the anomalous self-energy $\Sigma_{pp}(\mathbf{k}, \omega)$, which is identified as the SC gap, and therefore describes the strength of the electron pair. In this case, the dominant contribution to the strength of the electron pair arises from the sharp low-energy peaks both in $Re\Sigma_{pp}(\mathbf{k}_{AN}, \omega)$ and $Im\Sigma_{pp}(\mathbf{k}_{AN}, \omega)$ [82,83]. On the other hand, from the total self-energy in Eq. (4), the dressing of the electrons is mainly dominated by the normal self-energy $\Sigma_{ph}(\mathbf{k}_{AN}, \omega)$, indicating that the sharp low-energy peak in $Re\Sigma_{ph}(\mathbf{k}_{AN}, \omega)$ offsets mainly the single-electron band energy, while the sharp low-energy peak in $Im\Sigma_{ph}(\mathbf{k}_{AN}, \omega)$ governs mainly the lifetime of the quasiparticle excitation [83]. However, the sharp low-energy peak in the anomalous self-energy disappears in the normal state, while the sharp low-energy peak in the normal self-energy can persist into the normal state. This is also why the exotic features, including the intrinsic EFS reconstruction, the PDH structure in the quasiparticle excitation spectrum, the dispersion kink, and the ARPES autocorrelation and its connection with the quasiparticle scattering interference [59], arising from the dressing of the electrons that emerge in the SC-state, also appear in the normal state.

For a further understanding of the essential physics of the electron-doped cuprate superconductors, we have also studied the doping and momentum dependence of the low-

energy peak structures both in the normal and anomalous self-energies, and all the obtained results are consistent with the corresponding results obtained in the hole-doped counterparts [82,83]. We therefore complete the picture of the dressing of the electrons for the electron-doped cuprate superconductors, and we show the existence of the common origin of the anisotropic dressing of the electrons both in the electron- and hole-doped cuprate superconductors, i.e., the dressing of the electrons arises from the interaction of the electrons with a strongly dispersive spin excitation. Since the remarkable low-energy peak structures both in the normal and anomalous self-energies of the hole-doped cuprate superconductors [83] are well consistent with those deduced via machine learning "experiments" [82], we therefore predict that the similar low-energy peak structures both in the normal and anomalous self-energies can also be deduced from the experimental data of the ARPES spectra observed on the electron-doped cuprate superconductors in the proper annealing condition via machine learning.

## V. CONCLUSIONS

Within the framework of kinetic-energy-driven superconductivity, we have studied the phase diagram of electron-doped cuprate superconductors and the related exotic features of the anisotropic dressing of the electrons. Our results show that although the optimized $T_c$ in electron-doped superconductors is much smaller than that in their hole-doped counterparts, the electron- and hole-doped cuprate superconductors rather resemble each other in the doping range of the SC dome, indicating an absence of the disparity between the phase diagrams of the electron- and hole-doped cuprate superconductors. In particular, the anisotropic dressing of the electrons due to the strong electron coupling to a strongly dispersive spin excitation induces an EFS reconstruction, where the closed EFS

contour in the case without considering the strong electron interaction is broken up into the disconnected Fermi arcs centered around the nodal region, in qualitative agreement with the available experimental data. Moreover, we reveal the spin excitation effect in the quasiparticle excitation spectrum, where the dip in the PDH structure developed in the quasiparticle excitation spectrum at around the antinodal (nodal) region is directly related to the corresponding sharp peak in the antinodal (nodal) quasiparticle scattering rate, while the appearance of the dispersion kink is always associated with the emergence of the inflection point in the real part of the total self-energy and the sharp peak in the quasiparticle scattering rate. By comparing directly with the corresponding results in the hole-doped cuprate superconductors, our present results therefore show that the EFS reconstruction to form the Fermi arcs, the PDH structure in the quasiparticle excitation spectrum, and the dispersion kink are the intrinsic properties of both the electron- and hole-doped cuprate superconductors. Although some subtle differences between the electron- and hole-doped cuprate superconductors appear due to the electron-hole asymmetry, the coupling of the electrons with a strongly dispersive spin excitation is the common origin for the anisotropic dressing of the electrons both in the electron- and hole-doped cuprate superconductors. The theory also predicts that both the normal and anomalous self-energies exhibit notable low-energy peak-structures, which should be verified by future machine learning "experiments."

[1] J. G. Bednorz and K. A. Müller, Z. Phys. B **64**, 189 (1986).

[2] Y. Tokura, H. Takagi, and S. Uchida, Nature (London) **337**, 345 (1989).

[3] P. W. Anderson, Science **235**, 1196 (1987).

[4] See, e.g., M. Fujita, H. Hiraka, M. Matsuda, M. Matsuura, J. M. Tranquada, S. Wakimoto, G. Xu, and K. Yamada, J. Phys. Soc. Jpn. **81**, 011007 (2012).

[5] See, e.g., A. Damascelli, Z. Hussain, and Z.-X. Shen, Rev. Mod. Phys. **75**, 473 (2003).

[6] See, e.g., J. C. Campuzano, M. R. Norman, and M. Randeria, in *Physics of Superconductors*, edited by K. H. Bennemann and J. B. Ketterson (Springer, Berlin, 2004), Vol. II, p. 167.

[7] See, e.g., J. Fink, S. Borisenko, A. Kordyuk, A. Koitzsch, J. Geck, V. Zabalotnyy, M. Knupfer, B. Buechner, and H. Berger, in *Lecture Notes in Physics*, edited by S. Hüfner (Springer-Verlag, Berlin, 2007), Vol. 715, p. 295.

[8] See, e.g., N. P. Armitage, P. Fournier, and R. L. Greene, Rev. Mod. Phys. **82**, 2421 (2010).

[9] N. P. Armitage, D. H. Lu, C. Kim, A. Damascelli, K. M. Shen, F. Ronning, D. L. Feng, P. Bogdanov, Z.-X. Shen, Y. Onose, Y. Taguchi, Y. Tokura, P. K. Mang, N. Kaneko, and M. Greven, Phys. Rev. Lett. **87**, 147003 (2001).

[10] H. Matsui, K. Terashima, T. Sato, T. Takahashi, S.-C. Wang, H.-B. Yang, H. Ding, T. Uefuji, and K. Yamada, Phys. Rev. Lett. **94**, 047005 (2005).

[11] H. Matsui, K. Terashima, T. Sato, T. Takahashi, M. Fujita, and K. Yamada, Phys. Rev. Lett. **95**, 017003 (2005).

[12] H. Matsui, T. Takahashi, T. Sato, K. Terashima, H. Ding, T. Uefuji, and K. Yamada, Phys. Rev. B **75**, 224514 (2007).

[13] A. F. Santander-Syro, M. Ikeda, T. Yoshida, A. Fujimori, K. Ishizaka, M. Okawa, S. Shin, R. L. Greene, and N. Bontemps, Phys. Rev. Lett. **106**, 197002 (2011).

[14] D. Song, S. R. Park, C. Kim, Y. Kim, C. Leem, S. Choi, W. Jung, Y. Koh, G. Han, Y. Yoshida, H. Eisaki, D. H. Lu, Z.-X. Shen, and C. Kim, Phys. Rev. B **86**, 144520 (2012).

[15] T. Adachi, Y. Mori, A. Takahashi, M. Kato, T. Nishizaki, T. Sasaki, N. Kobayashi, and Y. Koike, J. Phys. Soc. Jpn. **82**, 063713 (2013).

[16] See, e.g., T. Adachi, T. Kawamata, and Y. Koike, Condens. Matter **2**, 23 (2017).

[17] M. Horio, T. Adachi, Y. Mori, A. Takahashi, T. Yoshida, H. Suzuki, L. C. C. Ambolode II, K. Okazaki, K. Ono, H. Kumigashira, H. Anzai, M. Arita, H. Namatame, M. Taniguchi, D. Ootsuki, K. Sawada, M. Takahashi, T. Mizokawa,

Y. Koike, and A. Fujimori, Nat. Commun. **7**, 10567 (2016).

[18] D. Song, G. Han, W. Kyung, J. Seo, S. Cho, Beom S. Kim, M. Arita, K. Shimada, H. Namatame, M. Taniguchi, Y. Yoshida, H. Eisaki, S. R. Park, and C. Kim, Phys. Rev. Lett. **118**, 137001 (2017).

[19] C. Lin, T. Adachi, M. Horio, T. Ohgi, M. A. Baqiya, T. Kawamata, H. Sato, T. Sumura, K. Koshiishi, S. Nakata, G. Shibata, K. Hagiwara, M. Suzuki, K. Ono, K. Horiba, H. Kumigashira, S. Ideta, K. Tanaka, Y. Koike, and A. Fujimori, arXiv:2006.04524.

[20] M. Horio, K. P. Kramer, Q. Wang, A. Zaidan, K. von Arx, D. Sutter, C. E. Matt, Y. Sassa, N. C. Plumb, M. Shi, A. Hanff, S. K. Mahatha, H. Bentmann, F. Reinert, S. Rohlf, F. K. Diekmann, J. Buck, M. Kalläne, K. Rossnagel, E. Rienks, V. Granata, R. Fittipaldi, A. Vecchione, T. Ohgi, T. Kawamata, T. Adachi, Y. Koike, A. Fujimori, M. Hoesch, and J. Chang, Phys. Rev. B **102**, 245153 (2020).

[21] I. Vekhter and C. M. Varma, Phys. Rev. Lett. **90**, 237003 (2003).

[22] See, e.g., J. P. Carbotte, T. Timusk, and J. Hwang, Rep. Prog. Phys. **74**, 066501 (2011).

[23] See, e.g., H.-Y. Choi and J. Mo Bok, Int. J. Mod. Phys. B **32**, 1840026 (2018).

[24] E. H. da S. Neto, P. Aynajian, A. Frano, R. Comin, E. Schierle, E. Weschke, A. Gyenis, J. Wen, J. Schneeloch, Z. Xu, S. Ono, G. Gu, M. Le Tacon, and A. Yazdani, Science **343**, 393 (2014).

[25] K. Fujita, C. K. Kim, I. Lee, J. Lee, M. H. Hamidian, I. A. Firmo, S. Mukhopadhyay, H. Eisaki, S. Uchida, M. J. Lawler, E.-A. Kim, and J. C. Davis, Science **344**, 612 (2014).

[26] See, e.g., I. M. Vishik, Rep. Prog. Phys. **81**, 062501 (2018).

[27] See, e.g., R. Comin and A. Damascelli, Annu. Rev. Condens. Matter Phys. **7**, 369 (2016).

[28] R. Comin, A. Frano, M. M. Yee, Y. Yoshida, H. Eisaki, E. Schierle, E. Weschke, R. Sutarto, F. He, A. Soumyanarayanan, Y. He, M. Le Tacon, I. S. Elfimov, J. E. Hoffman, G. A. Sawatzky, B. Keimer, and A. Damascelli, Science **343**, 390 (2014).

[29] D. S. Dessau, B. O. Wells, Z.-X. Shen, W. E. Spicer, A. J. Arko, R. S. List, D. B. Mitzi, and A. Kapitulnik, Phys. Rev. Lett. **66**, 2160 (1991).

[30] M. R. Norman, H. Ding, J. C. Campuzano, T. Takeuchi, M. Randeria, T. Yokoya, T. Takahashi, T. Mochiku, and K. Kadowaki, Phys. Rev. Lett. **79**, 3506 (1997).

[31] J. C. Campuzano, H. Ding, M. R. Norman, H. M. Fretwell, M. Randeria, A. Kaminski, J. Mesot, T. Takeuchi, T. Sato, T. Yokoya, T. Takahashi, T. Mochiku, K. Kadowaki, P. Guptasarma, D. G. Hinks, Z. Konstantinovic, Z. Z. Li, and H. Raffy, Phys. Rev. Lett. **83**, 3709 (1999).

[32] J. Wei, Y. Zhang, H. W. Ou, B. P. Xie, D. W. Shen, J. F. Zhao, L. X. Yang, M. Arita, K. Shimada, H. Namatame, M. Taniguchi, Y. Yoshida, H. Eisaki, and D. L. Feng, Phys. Rev. Lett. **101**, 097005 (2008).

[33] D. Mou, A. Kaminski, and G. Gu, Phys. Rev. B **95**, 174501 (2017).

[34] A. Kaminski, M. Randeria, J. C. Campuzano, M. R. Norman, H. Fretwell, J. Mesot, T. Sato, T. Takahashi, and K. Kadowaki, Phys. Rev. Lett. **86**, 1070 (2001).

[35] A. Lanzara, P. V. Bogdanov, X. J. Zhou, S. A. Kellar, D. L. Feng, E. D. Lu, T. Yoshida, H. Eisaki, A. Fujimori, K. Kishio,

[36] J.-I. Shimoyama, T. Noda, S. Uchida, Z. Hussain, and Z.-X. Shen, Nature (London) **412**, 510 (2001).

[36] A. A. Kordyuk, S. V. Borisenko, V. B. Zabolotnyy, J. Geck, M. Knupfer, J. Fink, B. Büchner, C. T. Lin, B. Keimer, H. Berger, A. V. Pan, S. Komiya, and Y. Ando, Phys. Rev. Lett. **97**, 017002 (2006).

[37] H. Iwasawa, J. F. Douglas, K. Sato, T. Masui, Y. Yoshida, Z. Sun, H. Eisaki, H. Bando, A. Ino, M. Arita, K. Shimada, H. Namatame, M. Taniguchi, S. Tajima, S. Uchida, T. Saitoh, D. S. Dessau, and Y. Aiura, Phys. Rev. Lett. **101**, 157005 (2008).

[38] N. C. Plumb, T. J. Reber, H. Iwasawa, Y. Cao, M. Arita, K. Shimada, H. Namatame, M. Taniguchi, Y. Yoshida, H. Eisaki, Y. Aiura, and D. S. Dessau, New J. Phys. **15**, 113004 (2013).

[39] S. Feng, L. Kuang, and H. Zhao, Physica C **517**, 5 (2015).

[40] D. Gao, Y. Liu, H. Zhao, Y. Mou, and S. Feng, Physica C **551**, 72 (2018).

[41] D. Gao, Y. Mou, and S. Feng, J. Low Temp. Phys. **192**, 19 (2018).

[42] D. Gao, Y. Mou, Y. Liu, S. Tan, and S. Feng, Philos. Mag. **99**, 752 (2019).

[43] Y. Liu, Y. Lan, Y. Mou, and S. Feng, Physica C **576**, 1353661 (2020).

[44] M. R. Norman, H. Ding, M. Randeria, J. C. Campuzano, T. Yokoya, T. Takeuchi, T. Takahashi, T. Mochiku, K. Kadowaki, P. Guptasarma, and D. G. Hinks, Nature (London) **392**, 157 (1998).

[45] A. Kanigel, U. Chatterjee, M. Randeria, M. R. Norman, S. Souma, M. Shi, Z. Z. Li, H. Raffy, and J. C. Campuzano, Phys. Rev. Lett. **99**, 157001 (2007).

[46] K. Nakayama, T. Sato, Y. Sekiba, K. Terashima, P. Richard, T. Takahashi, K. Kudo, N. Okumura, T. Sasaki, and N. Kobayashi, Phys. Rev. Lett. **102**, 227006 (2009).

[47] T. Kondo, A. D. Palczewski, Y. Hamaya, T. Takeuchi, J. S. Wen, Z. J. Xu, G. Gu, and A. Kaminski, Phys. Rev. Lett. **111**, 157003 (2013).

[48] U. Chatterjee, M. Shi, A. Kaminski, A. Kanigel, H. M. Fretwell, K. Terashima, T. Takahashi, S. Rosenkranz, Z. Z. Li, H. Raffy, A. Santander-Syro, K. Kadowaki, M. R. Norman, M. Randeria, and J. C. Campuzano, Phys. Rev. Lett. **96**, 107006 (2006).

[49] Y. He, Y. Yin, M. Zech, A. Soumyanarayanan, M. M. Yee, T. Williams, M. C. Boyer, K. Chatterjee, W. D. Wise, I. Zeljkovic, T. Kondo, T. Takeuchi, H. Ikuta, P. Mistark, R. S. Markiewicz, A. Bansil, S. Sachdev, E. W. Hudson, and J. E. Hoffman, Science **344**, 608 (2014).

[50] See, e.g., P. A. Lee, N. Nagaosa, and X.-G. Wen, Rev. Mod. Phys. **78**, 17 (2006).

[51] See, e.g., B. Edegger, V. N. Muthukumar, and C. Gros, Adv. Phys. **56**, 927 (2007).

[52] M. S. Hybertsen, E. B. Stechel, M. Schluter, and D. R. Jennison, Phys. Rev. B **41**, 11068 (1990).

[53] R. J. Gooding, K. J. E. Vos, and P. W. Leung, Phys. Rev. B **50**, 12866 (1994).

[54] C. Kim, P. J. White, Z.-X. Shen, T. Tohyama, Y. Shibata, S. Maekawa, B. O. Wells, Y. J. Kim, R. J. Birgeneau, and M. A. Kastner, Phys. Rev. Lett. **80**, 4245 (1998).

[55] S. Feng, J. Qin, and T. Ma, J. Phys.: Condens. Matter **16**, 343 (2004); S. Feng, Z. B. Su, and L. Yu, Phys. Rev. B **49**, 2368 (1994).

[56] See, e.g., S. Feng, Y. Lan, H. Zhao, L. Kuang, L. Qin, and X. Ma, Int. J. Mod. Phys. B **29**, 1530009 (2015).

[57] S. Feng, Phys. Rev. B **68**, 184501 (2003); S. Feng, T. Ma, and H. Guo, Physica C **436**, 14 (2006).

[58] S. Feng, H. Zhao, and Z. Huang, Phys. Rev. B **85**, 054509 (2012); S. Feng, *ibid.* **85**, 099902(E) (2012).

[59] S. Tan, Y. Mou, Y. Liu, and S. Feng, J. Supercond. Novel Magn. **33**, 2305 (2020); Mod. Phys. Lett. B **34**, 2040053 (2020).

[60] G. M. Eliashberg, Sov. Phys. JETP **11**, 696 (1960).

[61] J. L. Tallon, C. Bernhard, H. Shaked, R. L. Hitterman, and J. D. Jorgensen, Phys. Rev. B **51**, 12911 (1995).

[62] T. Adachi, A. Takahashi, K. M. Suzuki, M. A. Baqiya, T. Konno, T. Takamatsu, M. Kato, I. Watanabe, A. Koda, M. Miyazaki, R. Kadono, and Y. Koike, J. Phys. Soc. Jpn. **85**, 114716 (2016).

[63] S. R. Park, Y. S. Roh, Y. K. Yoon, C. S. Leem, J. H. Kim, B. J. Kim, H. Koh, H. Eisaki, N. P. Armitage, and C. Kim, Phys. Rev. B **75**, 060501(R) (2007).

[64] I. A. Nekrasov, N. S. Pavlov, E. Z. Kuchinskii, M. V. Sadovskii, Z. V. Pchelkina, V. B. Zabolotnyy, J. Geck, B. Büchner, S. V. Borisenko, D. S. Inosov, A. A. Kordyuk, M. Lambacher, and A. Erb, Phys. Rev. B **80**, 140510(R) (2009).

[65] M. Ikeda, T. Yoshida, A. Fujimori, M. Kubota, K. Ono, H. Das, T. Saha-Dasgupta, K. Unozawa, Y. Kaga, T. Sasagawa, and H. Takagi, Phys. Rev. B **80**, 014510 (2009).

[66] M. Ikeda, T. Yoshida, A. Fujimori, M. Kubota, K. Ono, Y. Kaga, T. Sasagawa, and H. Takagi, Phys. Rev. B **80**, 184506 (2009).

[67] J. W. Harter, L. Maritato, D. E. Shai, E. J. Monkman, Y. Nie, D. G. Schlom, and K. M. Shen, Phys. Rev. Lett. **109**, 267001 (2012).

[68] J. W. Harter, L. Maritato, D. E. Shai, E. J. Monkman, Y. Nie, D. G. Schlom, and K. M. Shen, Phys. Rev. B **92**, 035149 (2015).

[69] K. Tanaka, T. Yoshida, A. Fujimori, D. H. Lu, Z.-X. Shen, X.-J. Zhou, H. Eisaki, Z. Hussain, S. Uchida, Y. Aiura, K. Ono, T. Sugaya, T. Mizuno, and I. Terasaki, Phys. Rev. B **70**, 092503 (2004).

[70] C. T. Shih, T. K. Lee, R. Eder, C.-Y. Mou, and Y. C. Chen, Phys. Rev. Lett. **92**, 227002 (2004).

[71] E. Pavarini, I. Dasgupta, T. Saha-Dasgupta, O. Jepsen, and O. K. Andersen, Phys. Rev. Lett. **87**, 047003 (2001).

[72] See, e.g., G. D. Mahan, *Many-Particle Physics* (Plenum, New York, 1981).

[73] E. H. da Silva Neto, R. Comin, F. He, R. Sutarto, Y. Jiang, R. L. Greene, G. A. Sawatzky, and A. Damascelli, Science **347**, 282 (2015).

[74] E. H. da Silva Neto, B. Yu, M. Minola, R. Sutarto, E. Schierle, F. Boschini, M. Zonno, M. Bluschke, J. Higgins, Y. Li, G. Yu, E. Weschke, F. He, M. Le Tacon, R. L. Greene, M. Greven, G. A. Sawatzky, B. Keimer and A. Damascelli, Sci. Adv. **2**, e1600782 (2016).

[75] Y. Mou and S. Feng, Philos. Mag. **97**, 3361 (2017).

[76] I. M. Vishik, E. A. Nowadnick, W. S. Lee, Z. X. Shen, B. Moritz, T. P. Devereaux, K. Tanaka, T. Sasagawa, and T. Fujii, Nat. Phys. **5**, 718 (2009).

[77] M. Horio, S. Sakai, K. Koshiishi, Y. Nonaka, H. Suzuki, J. Xu, M. Hashimoto, D. Lu, Z.-X. Shen, T. Ohgi, T. Konno, T. Adachi, Y. Koike, M. Imada, and A. Fujimori, arXiv:1801.04247.

[78] A. F. Santander-Syro, T. Kondo, J. Chang, A. Kaminski, S. Pailhes, M. Shi, L. Patthey, A. Zimmers, B. Liang, P. Li, and R. L. Greene, arXiv:0903.3413.

[79] F. Schmitt, W. S. Lee, D.-H. Lu, W. Meevasana, E. Motoyama, M. Greven, and Z.-X. Shen, Phys. Rev. B **78**, 100505(R) (2008).

[80] S. R. Park, D. J. Song, C. S. Leem, C. Kim, C. Kim, B. J. Kim, and H. Eisaki, Phys. Rev. Lett. **101**, 117006 (2008).

[81] N. P. Armitage, D. H. Lu, C. Kim, A. Damascelli, K. M. Shen, F. Ronning, D. L. Feng, P. Bogdanov, X. J. Zhou, W. L. Yang, Z. Hussain, P. K. Mang, N. Kaneko, M. Greven, Y. Onose, Y. Taguchi, Y. Tokura, and Z.-X. Shen, Phys. Rev. B **68**, 064517 (2003).

[82] Y. Yamaji, T. Yoshida, A. Fujimori, and M. Imada, arXiv:1903.08060.

[83] Y. Liu, Yu Lan, and S. Feng, arXiv:2004.06489.